

# Record Fifth-Harmonic-Generation Efficiency Producing 211-nm, Joule-Level Pulses Using Cesium Lithium Borate

## Introduction

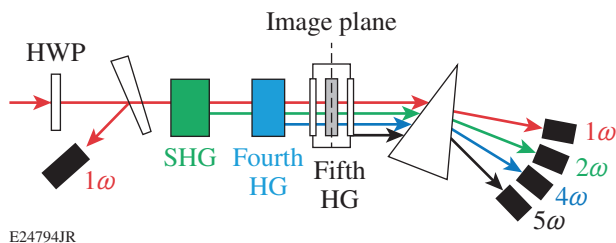
High-energy ultraviolet (UV) sources are now required to probe hot dense plasmas, where deep UV probes provide a better penetration of the plasma.<sup>1</sup> For fusion experiments, measuring Thomson scattering of  $5\omega$  pulses as a diagnostic technique is promising because there is less self-generated background from the plasma in the spectral region from 180 to 230 nm (Refs. 2 and 3). More generally, all-solid-state UV lasers can address applications traditionally supported by excimer gas lasers.<sup>4</sup>

Fifth-harmonic generation (5HG) of neodymium lasers was first demonstrated in 1969 (Ref. 5) using a KDP (potassium dihydrogen phosphate) crystal to mix the fourth harmonic with the residual beam at the fundamental frequency:  $4\omega + \omega = 5\omega$ . ADP (ammonium dihydrogen phosphate) crystals were later used in a similar configuration.<sup>6–8</sup> Both KDP and ADP crystals must be cooled to cryogenic temperatures in order for this process to be phase matched. Fifth-harmonic generation was achieved at room temperature using crystals of potassium pentaborate tetrahydrate (KB5),<sup>9,10</sup> urea,<sup>11</sup>  $\beta$ -barium borate (BBO),<sup>12</sup> and cesium lithium borate (CLBO).<sup>13</sup> All of these experiments used small-aperture beams and had relatively low efficiency. As a result, real applications of 5HG have been rare.<sup>14</sup>

Although common crystals such as BBO have been used to generate the fifth harmonic,<sup>15</sup> joule-level applications require crystals that can be grown to sizes suitable for large-aperture beams (~25 mm or greater). KDP and ADP crystals can be grown in meter-scale sizes; the 20%-efficient 5HG of wide-aperture neodymium glass was first reported in an ADP crystal.<sup>16</sup> However, maintaining a cryogenic temperature with sub-degree-Kelvin uniformity throughout the ADP crystal, as required for phase matching, adds significant complexity for large-aperture applications.<sup>17</sup> Another candidate is CLBO, which can also be grown in large sizes.<sup>13</sup> In this article we demonstrate 30%-efficient, joule-class fifth-harmonic conversion of 1053-nm pulses using a 30-mm-diam CLBO crystal.

## Experiment

Figure 153.11 shows the experimental setup with the cascade of three nonlinear crystals. The final crystal, made of CLBO, was located at the image plane of a Nd:YLF laser<sup>18</sup> that was optimized to produce a flattopped, square-beam profile with a square pulse (1053 nm,  $12 \times 12$  mm, from 1 ns to 2.8 ns,  $\leq 1.5$  J, 5 Hz or 0.1 Hz). The first frequency doubler was a deuterated potassium dihydrogen phosphate (DKDP) crystal, which was chosen instead of KDP to decrease linear absorption at the fundamental frequency. It was cut in a Type-II configuration ( $30 \times 30 \times 27$  mm) to convert  $1\omega \rightarrow 2\omega$ . A second frequency doubler, a Type-I KDP crystal ( $30 \times 30 \times 15.5$  mm), was used to convert  $2\omega \rightarrow 4\omega$ .



E24794JR

Figure 153.11

Experimental setup showing the input laser beam, conversion crystals, and energy diagnostics for each frequency: second-harmonic generation (SHG) in deuterated potassium dihydrogen phosphate (DKDP), Type II; fourth-harmonic generation (4HG) in KDP, Type I; and fifth-harmonic generation (5HG) in cesium lithium borate (CLBO), Type I. HWP: half-wave plate.

A CLBO crystal from Coherent (30-mm diam  $\times$  4 mm), which was cut for Type-I phase-matching conversion, mixed the residual  $1\omega$  with the  $4\omega$  to produce  $5\omega$  pulses. Because of its hygroscopic properties, it was housed in an oven and heated to  $120^\circ\text{C}$ . The crystal orientations relative to the input beam polarization are shown in Fig. 153.12. The angle  $\alpha$  between input-beam polarization and the horizontal plane was tuned using the half-wave plate (HWP) before the first crystal to change the balance of energy between the ordinary and extraordinary axes in the first Type-II doubler and to preserve some fraction of the fundamental frequency beam through

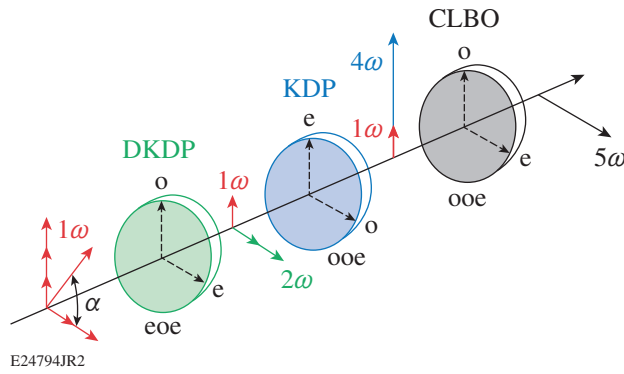


Figure 153.12 Schematic showing the orientation of the crystal axes and polarizations. The angle ( $\alpha$ ) of the  $1\omega$  polarization was set using a HWP for optimal conversion. e: extraordinary; o: ordinary.

the first two crystals for the interaction in the last crystal. The input and output beam energies were measured using identical pyroelectric energy meters that were cross calibrated. All beam profiles were recorded.

## Results

Frequency conversion efficiencies from  $1\omega \rightarrow 2\omega$  and  $2\omega \rightarrow 4\omega$  are shown in Fig. 153.13 and demonstrate a good agreement with plane-wave conversion calculations. For the doubling calculation, we assumed an effective nonlinearity of  $0.31 \text{ pm/V}$  for the DKDP Type-II doubler, an angular detuning of  $200 \mu\text{rad}$  (internal angle) from phase matching, and an equal split of  $1\omega$  input into the two polarization axes of the doubler crystal. For the quadrupling calculation, a Type-I KDP quadrupling crystal

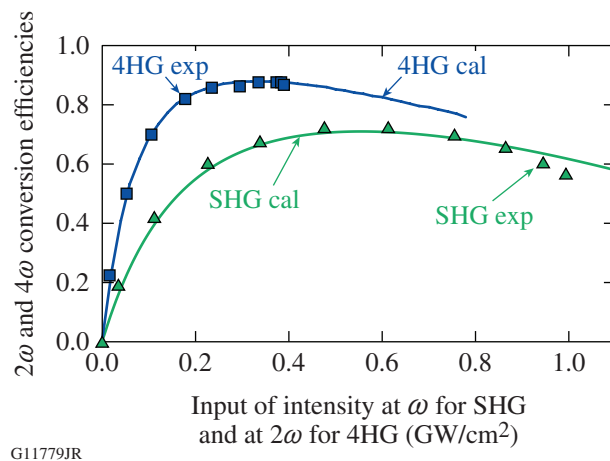


Figure 153.13 SHG and 4HG efficiencies measured as a function of input-pulse intensity.

is assumed to have an effective nonlinearity of  $0.45 \text{ pm/V}$  with an angular detuning of  $50 \mu\text{rad}$ .

To maximize the  $5\omega$  output energy, the efficiency of the second-harmonic-generation (SHG) process was lowered to preserve some portion of energy at fundamental frequency for the  $(1\omega + 4\omega)$  process. The maximum of  $5\omega$  energy reached with a 2.4-ns pulse was 335 mJ.

The fifth-harmonic efficiency  $\eta(5\omega)$ , shown in Fig. 153.14, is defined as the ratio of  $5\omega$  output energy after the CLBO oven to the  $1\omega$  energy at the input of the first (DKDP) crystal. The maximum  $\eta(5\omega)$  conversion efficiency of 30.5% was reached with a 2.4-ns pulse and an input intensity of  $0.3 \text{ GW/cm}^2$ . This definition of efficiency describes the portion of the input  $1\omega$  energy that has been transformed into the fifth harmonic and is available at the output of the cascade of crystals for use in any application. However, this definition depends on technical factors not directly related to the performance of the CLBO crystal, such as the quality of antireflection coatings on all of the crystals and oven windows, absorption in the first two doubling crystals, etc.; therefore, this efficiency metric does not provide an accurate description of the physics of the mixing  $(1\omega + 4\omega)$  process. Other publications have proposed alternate methods to calculate 5HG efficiency such as the fraction ratio (FR) of  $5\omega$  energy after the last crystal to the total energy output at all wavelengths,<sup>16</sup> or as a ratio of  $5\omega$  energy after the last crystal to the  $1\omega$  energy at the input of the last crystal.<sup>15</sup> A quantum efficiency (QE) for the process can be defined as the ratio of the number of photons after all the crystals,  $5\omega$  to  $(4\omega + 5\omega)$ ,

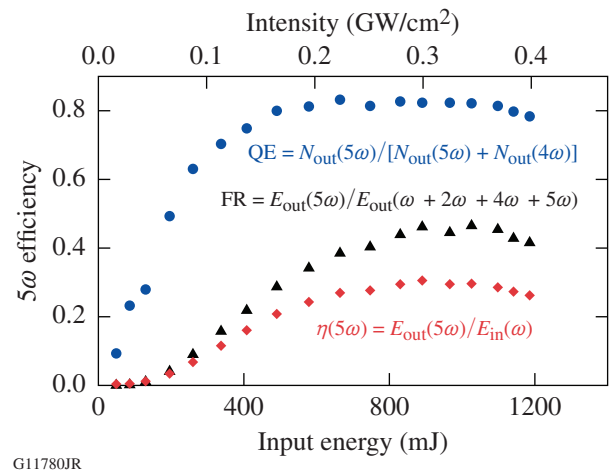
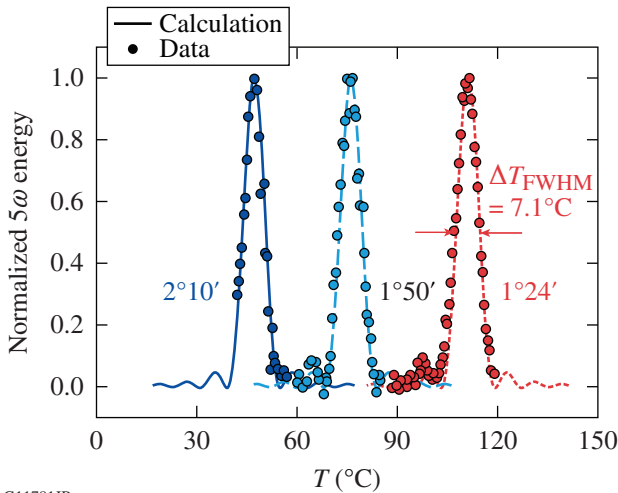


Figure 153.14 Measurement of 5HG efficiencies according to three definitions.

which has an ideal value of 100% when all  $4\omega$  photons are converted into  $5\omega$  photons. The best QE that was observed in this experiment exceeded 80%; i.e., despite the complexity of the interaction, four of the five photons of  $4\omega$  were converted.

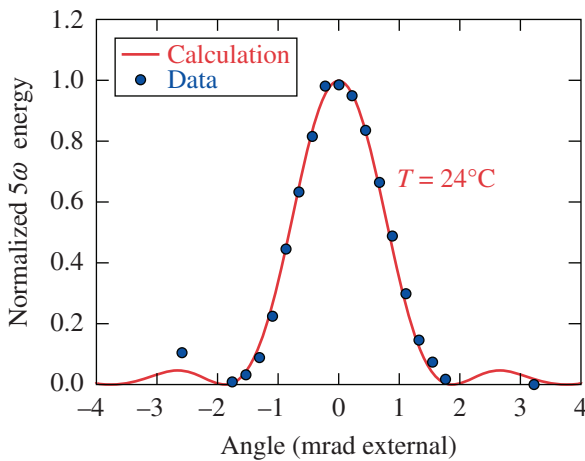
The temperature acceptance of 5HG in CLBO at three different crystal position angles was measured (see Fig. 153.15). Angular acceptance of 5HG at a given temperature of the CLBO crystal was also measured (Fig. 153.16). The measured acceptances agree well with the simulations.

The 5HG energy was optimized by adjusting the angle  $\alpha$  to set  $1\omega$  intensity at the CLBO for a 1-ns pulse (see Fig. 153.17).



G11781JR

Figure 153.15 Fifth-harmonic energy temperature ( $T$ ) acceptance at three different position angles of the CLBO crystal. FWHM: full width at half maximum.

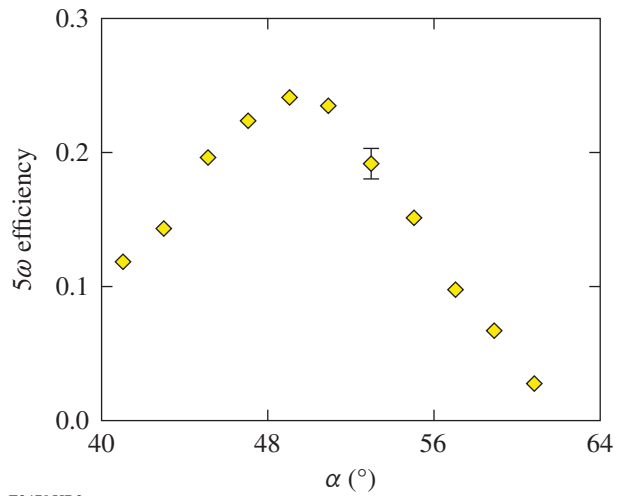


G11782JR

Figure 153.16 Fifth-harmonic energy angular acceptance of the CLBO crystal.

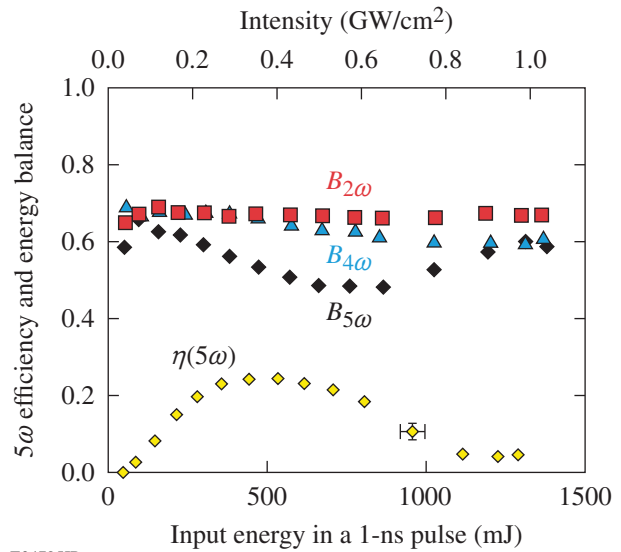
The optimal angle depends on input-beam intensity, so fine tuning should be done close to the range of the best  $5\omega$  generation.

Figure 153.18 shows quantities derived from energy measurements plotted as a function of input energy and intensity with a 1-ns pulse. In addition to the fifth-harmonic efficiency  $\eta(5\omega)$ , which is defined above, the figure shows the energy balance  $B$ , which is the ratio of the total energy of all beams



E24795JR2

Figure 153.17 Fifth-harmonic efficiency as a function of input polarization direction.



E24795JR

Figure 153.18 Fifth-harmonic efficiency and energy balance measured as a function of input-pulse energy and intensity.  $B_{2\omega}$ ,  $B_{4\omega}$ , and  $B_{5\omega}$  are the energy balances measured by phase matching the crystals for a maximum frequency of  $2\omega$ ,  $4\omega$ , and  $5\omega$ , respectively.

after the oven to the  $1\omega$  energy at the input;  $B$ , therefore, represents the fraction of energy transmitted from input to output. The subscript denotes the maximum harmonic frequency present, which was set by detuning crystals to suppress  $5\omega$  or  $4\omega$  generation.

A  $5\omega$  conversion efficiency of 25% was reached with a 1-ns pulse and an input intensity of 0.4 GW/cm<sup>2</sup>. Strong back-conversion occurred at higher intensities, reducing the overall efficiency. The energy balance  $B$  at low intensities was only 70%, primarily caused by losses from uncoated surfaces of the CLBO and the output oven window, and  $1\omega$  reflections from the KDP crystal surfaces. It is expected that the overall  $5\omega$  efficiency could be significantly improved by reducing these losses.

The variation in energy balance at higher intensities shows that nonlinear loss mechanisms are also present. While the  $4\omega$  and  $5\omega$  photon energies are below the band gap of CLBO, any combination of the two [( $4\omega + 4\omega$ ), ( $4\omega + 5\omega$ ), and ( $5\omega + 5\omega$ )] exceeds the band gap and initiates two-photon absorption (TPA) in CLBO. This nonlinear process dominates at a high intensity and becomes the most-limiting factor for efficient 5HG. By detuning the crystals to suppress  $5\omega$  or  $4\omega$  generation, the relative significance of two-photon absorption of  $4\omega$  and  $5\omega$  light was determined. With all crystals optimized ( $B_{5\omega}$ ), any combination of TPA can occur, but with the CLBO crystal detuned ( $B_{4\omega}$ ), only ( $4\omega + 4\omega$ ) is relevant. The difference between the three energy balance curves shows that TPA from ( $4\omega + 5\omega$ ) and ( $5\omega + 5\omega$ ) is the main nonlinear loss mechanism, whereas the ( $4\omega + 4\omega$ ) process is relatively weak. TPA coefficients  $\beta$  at  $5\omega$  measured in the CLBO crystal, in a UV-grade fused-silica window, and in air are 1.2 cm/GW, 0.5 cm/GW, and 0.0008 cm/GW, respectively.

Another factor that limits 5HG is the temperature non-uniformity across the CLBO crystal. Figure 153.19 shows beam profiles of the input beam before the first crystals and fifth-harmonic beam after the oven. Compared to the relatively uniform  $1\omega$  beam, the  $5\omega$  beam varied spatially and was significantly smaller. By temperature tuning, the optimal zone of  $5\omega$  generation could be moved vertically across the CLBO crystal, demonstrating that the nonuniformity of the  $5\omega$  beam was caused by phase mismatch inside the CLBO crystal. Independent temperature measurements also demonstrated a similar thermal gradient of the CLBO crystal inside the oven. Therefore, improving an oven to produce a more-uniform temperature across the CLBO crystal would increase the  $5\omega$  generation efficiency beyond 30%.

ACKNOWLEDGMENT

This material is based upon work supported by the Department of Energy National Nuclear Security Administration under Award Number DE-NA0001944, the University of Rochester, and the New York State Energy Research and Development Authority.

REFERENCES

1. V. V. Ivanov, A. A. Anderson, and I. A. Begishev, *Appl. Opt.* **55**, 498 (2016).
2. J. S. Ross, S. H. Glenzer, J. P. Palastro, B. B. Pollock, D. Price, G. R. Tynan, and D. H. Froula, *Rev. Sci. Instrum.* **81**, 10D523 (2010).
3. P. Datte, J. S. Ross, D. Froula, J. Galbraith, S. Glenzer, B. Hatch, J. Kilkenny, O. Landen, A. M. Manuel, W. Molander, D. Montgomery, J. Moody, G. Swadling, J. Weaver, G. Vergel de Dios, and M. Vitalich, *J. Phys.: Conf. Ser.* **717**, 012089 (2016).
4. *Excimer Laser Technology*, edited by D. Basting and G. Marowsky (Springer-Verlag, Berlin, 2005).

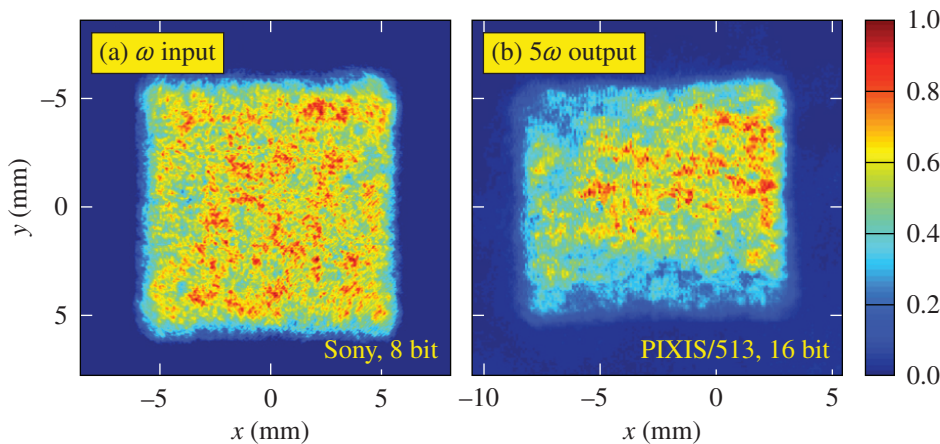


Figure 153.19  
(a) Input beam at the fundamental frequency on the front of the cascade of crystals and (b) fifth-harmonic output beam after the oven.

G11783JR

5. A. G. Akmanov *et al.*, J. Exp. Theor. Phys. Lett. **10**, 154 (1969).
6. G. A. Massey, Appl. Phys. **24**, 371 (1974).
7. G. Massey, M. Jones, and J. Johnson, IEEE J. Quantum Electron. **14**, 527 (1978).
8. M. Jones and G. Massey, IEEE J. Quantum Electron. **15**, 204 (1979).
9. K. Kato, Opt. Commun. **19**, 332 (1976).
10. A. G. Arutyunyan *et al.*, Sov. Tech. Phys. Lett. **6**, 120 (1980).
11. K. Kato, IEEE J. Quantum Electron. **QE-16**, 810 (1980).
12. C. Chen *et al.*, Proc. SPIE **681**, 12 (1986).
13. Y. K. Yap *et al.*, Opt. Lett. **21**, 1348 (1996).
14. A. Lago *et al.*, Opt. Lett. **13**, 221 (1988).
15. A. Dubietis *et al.*, J. Opt. Soc. Am. B **17**, 48 (2000).
16. I. A. Begishev, R. A. Ganeev, A. A. Gulamov, E. A. Erofeev, Sh. R. Kamalov, T. Usmanov, and A. D. Khadzhaev, Sov. J. Quantum Electron. **18**, 224 (1988).
17. I. A. Begishev, R. A. Ganeev, V. V. Gorbushin, A. A. Gulamov, Sh. R. Kamalov, and T. Usmanov, J. Appl. Spectrosc. **51**, 1218 (1989).
18. V. Bagnoud, M. J. Guardalben, J. Puth, J. D. Zuegel, T. Mooney, and P. Dumas, Appl. Opt. **44**, 282 (2005).